Computers and Fluids 148 (2017) 10–25

Contents lists available at ScienceDirect

Computers and Fluids

journal homepage: www.elsevier.com/locate/compfluid

Numerical modelling of the rise of Taylor bubbles through a change in pipe diameter

Stephen Ambrose, Ian S. Lowndes, David M. Hargreaves*, Barry Azzopardi

Faculty of Engineering, University of Nottingham, Nottingham, NG7 2RD, UK

ARTICLE INFO

Article history:
Received 9 August 2016
Revised 23 January 2017
Accepted 28 January 2017
Available online 11 February 2017

Keywords:
Numerical simulation
Taylor bubble
Change in geometry
Oscillations
CFD

ABSTRACT

The rise of Taylor bubbles through expansions in vertical pipes is modelled using Computational Fluid Dynamics. The predictions from the models are compared against existing experimental work and show good agreement, both quantitatively and qualitatively. Many workers, including the present work, find that, as the bubble passes through the expansion, it will either remain intact or split into one or more daughter bubbles. We find that the critical length of bubble, defined as the maximum length that will pass through intact, is proportional to the cosecant of the angle of the expansion. Further, we show that for an abrupt expansion, the critical bubble length became unaffected by the walls of the upper pipe as the diameter was increased.

1. Introduction

The rise of Taylor bubbles is a well–documented and well–studied phenomenon in many fields, from chemical reactions in micro-scale systems to the eruption of volcanoes. Taylor bubbles are elongated, bullet-shaped gas bubbles that move through stagnant or co-flowing liquid in horizontal, inclined or, in the present context, vertical pipes (Fig. 1). Research in this field has focussed in a variety of topics, in particular the characterisation of the rise rate of the bubbles [9,27], the determination of the flow fields ahead of Nogueira et al. [20], in the liquid film around [4] and in the wake region behind the bubble [21]. Despite these and numerous other studies, there is a paucity of published experimental or numerical work on Taylor bubbles that encounter a change in pipe diameter as they rise.

James et al. [12] reported the results of an experimental investigation into the rise single Taylor bubbles through a variety of pipe expansions and contractions (using 0.038, 0.05 and 0.08 m diameter pipe sections). Sugar syrup solutions of different concentrations, with viscosities of 0.001, 0.1 and 30 Pa s, were used to compare the rise behaviour across a range of Froude numbers. These experiments were monitored quantitatively by means of pressure sensors and force meters and also qualitatively by video recording. They observed that when a Taylor bubble encountered an expansion in pipe diameter, it rapidly expanded both vertically and laterally from the nose. It was hypothesised that this resulted in an increase in the flow in the liquid film surrounding the bubble which caused the observed necking or pinching of the bubble. For bubbles above a certain length, this necking process splits the bubble into two or more daughter bubbles as shown in Fig. 2, which is a schematic of the process taken from James et al. [12]. The splitting will also generate oscillations in the pressure, which they measured both above and below the expansion. The objective of their work was to compare the experimental pressure signals measured against the acoustic seismic data recorded at active volcanic sites; their hypothesis being that the source of pressure oscillations observed in seismic data are caused by a large bubble of gas rising through a sudden expansion in the cross-sectional area of the conduit. They were able to show that the pressure changes measured during in their experiments exhibited similar behaviour to those recorded in the field, hence adding weight to their hypothesis.

Kondo et al. [16], whose primary focus was on co-current bubbly liquid gas flow, conducted a number of experiments using single Taylor bubbles in a quiescent liquid. In these, a Taylor bubble rises through a pipe of diameter 0.02 m which undergoes a sudden expansion to one with a diameter of 0.05 m. Fig. 3 shows a still video image taken from Kondo et al. [16] showing the bubble during the necking process–the poor quality is due to the standard of photocopy available. After the neck of the bubble closes, the rear of the leading bubble bursts through the nose of that part of the bubble. This process can be observed in the still video images shown in Fig. 4. These images have been taken after the sudden expansion but are cropped to the central 0.02 m of the pipe.

* Corresponding author.
E-mail address: david.hargreaves@nottingham.ac.uk (D.M. Hargreaves).

http://dx.doi.org/10.1016/j.compfluid.2017.01.023

Fig. 1. Examples of an air Taylor bubble rising through (a) water and (b) silicone oil [7].

Danabalan [8] investigated the rise of Taylor bubbles as they move from a straight, vertical pipe into either a rounded glass bowl or else a cubic box–the rationale being that this is an analogue of a conduit in a volcano expanding into a lava lake. One novel aspect of the work was that she looked for the maximum volume of bubble that could pass through the expansion without breaking into two or more daughter bubbles. It was found that the critical volume at which this splitting occurred was dependent on the viscosity of the liquid and the geometry of the expansion, with the rounded glass bowl being able to support a larger bubble passing through intact. Notice that in Fig. 5 there is no evidence of the bursting of the bubble from behind as was reported by Kondo et al. [16]. This is due to the much higher viscosity of the liquid in Danabalan's work.

Another experimental study recently conducted by Soldati [24] employed a Hele-Shaw cell to investigate the effect of the angle of expansion, fluid viscosity and volume of bubble may have on the rise characteristics. A Hele-Shaw cell is made up of two parallel plates some distance apart which are sealed at the sides. By varying the volume of air injected into the base of the apparatus, different lengths of Taylor bubbles were generated in the cell and it was possible to find the critical volume of bubble which can pass through the expansion without splitting by the necking of the bubble. Similar to approach of Danabalan [8], an exact value for the critical length could not be found, but only upper and lower bounds for it. Thus the critical bubble volume was deemed to lie between a lower volume, which could pass through the expansion unbroken, and an upper volume, when the bubble did break up.

Fig. 3. A still video image extracted and cleaned-up from Kondo et al. [16] which shows a Taylor bubble during the necking process while passing through a sudden expansion from a pipe of diameter 0.02 m to 0.05 m in water.

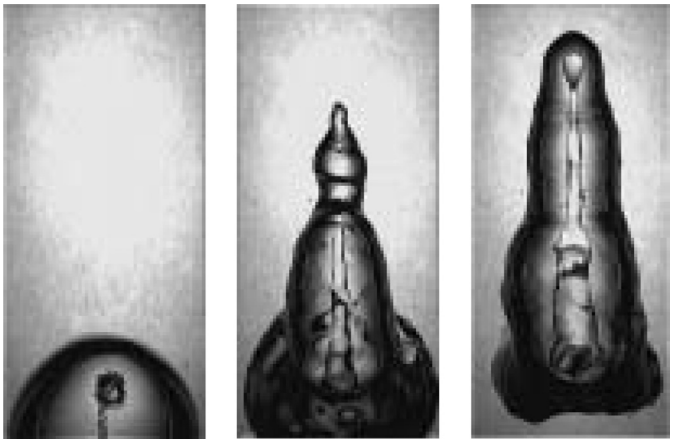

Fig. 4. A series of still video images extracted from Kondo et al. [16] which show a Taylor bubble which has passed through a sudden expansion from a pipe of diameter 0.02 m to 0.05 m in water.

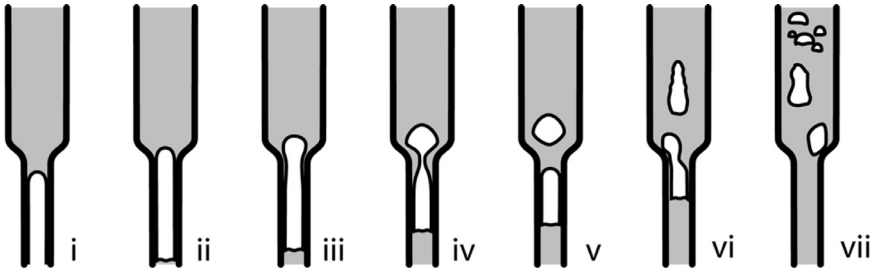

Fig. 2. Sketches of the breakup of a long parent bubble into several daughter bubbles [12].

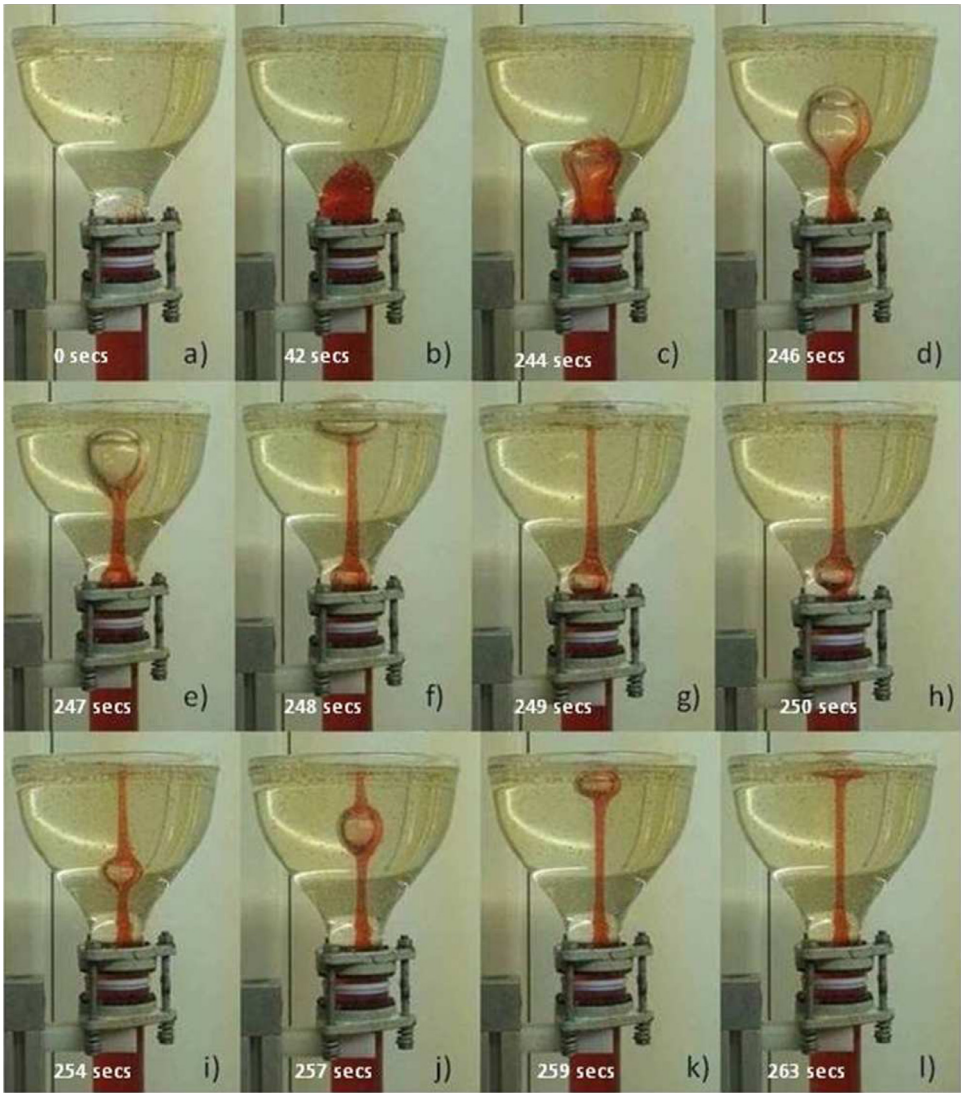

Fig. 5. A photographic sequence of a 60 cm^3 Taylor bubble injected into a liquid with viscosity of 68 Pa s moving into a rounded bowl [8]. The upper bowl is filled with clear glucose syrup and the lower pipe is filled with glucose syrup mixed with red dye. Images (a) to (f) show the passage of the first daughter bubble while (g) to (l) shows a second daughter bubble rising after a brief hiatus. (For interpretation of the references to colour in this figure legend, the reader is referred to the web version of this article.)

Soldati [24] concludes that the critical length of a bubble decreases as the angle of expansion, θ, (for a definition of θ, see Fig. 7) increases from 30° to 90°, as shown in Fig. 6. This is consistent with the findings of Danabalan [8], in which a 90° expansion gave a smaller critical length than a more gradual increase in pipe diameter. In Fig. 6 the filled circles indicate the bubbles which did not break up as they rose through the expansion, whilst the unfilled circles indicate those that did.

Fig. 7, taken from Soldati [24], shows a series of diagrams based on still photographs that clearly illustrate the different stages of the breakup mechanism. As the nose of the bubble enters the expansion section of the pipe, the nose of the bubble expands to fill the widening diameter as it is no longer constrained by the channel walls of the lower pipe section. As the nose of the bubble expands, the middle of the bubble thins out. If the bubble is longer than the critical length, it will break into two parts, as shown in Fig. 7(d) and (e).

Recently, Carter et al. [5] studied the acoustic signals produced by the breakup of a Taylor bubble as it rises through an expansion in the pipe diameter. The experimental apparatus used in this study consisted of a 0.01 m diameter pipe concentrically mounted inside a longer 0.025 m diameter pipe - not strictly an expansion in the terms we have defined previously, but a change in cross-sectional area nonetheless. Both were filled with water and a specified volume of air was injected into the inner pipe while a high speed camera was used to record the behaviour of the bubbles. A high sensitivity microphone was located above the surface of the water to record the acoustic signals generated. Although no significant conclusions could be drawn from an analysis of the acoustic signals, an analysis of the high speed camera images gave further qualitative insight into the process of the breakup mechanism of a Taylor bubble passing through an expansion (Fig. 8).

In the figure, the negatives of still images extracted from a high speed video recording of a Taylor bubble rising in water through an expansion are shown. The time between successive images is 20 ms. Images (a) to (d) show the bubble starting to neck as water is entrained from the outer pipe. As the bubble continues to neck a fine central tube of air is maintained, shown in image (e). From there, image (f), this film breaks and water is catapulted through the centre of the upper bubble, forming a “spike”, similar to that seen in Fig. 4. This then penetrates the nose of the bubble and water jets through this opening, which is shown in images (g). Carter

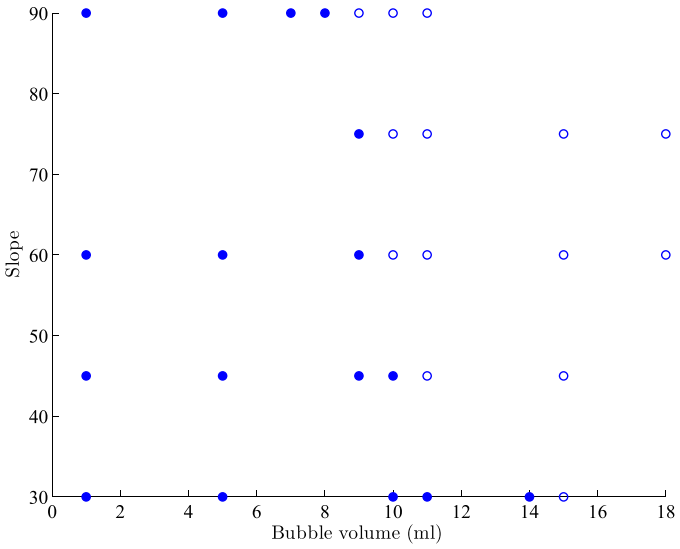

Fig. 6. A diagram showing Taylor bubble breakup or otherwise for different angles of expansion (adapted from Soldati [24]). Solid markers indicate bubbles that did not break up, hollow markers those that did.

et al. [5] also reported extensively on the size of the daughter bubble released from the tube. If the parent bubble were large enough, they found that a series of daughter bubbles may be released.

In this paper we use commercial Computational Fluid Dynamics (CFD) software to model and gain a better understanding of the behaviour of Taylor bubbles rising through changes in pipe geometry. To our knowledge, there have been no published computational studies of Taylor bubbles rising through expansions in pipe diameter.

There do exist, however, several CFD studies investigating the rise of Taylor bubbles, either in stagnant fluid or co-current conditions, but these have focussed on straight vertical or inclined pipes. Some have used a bubble-centred reference frame, whereby the walls of the domain are moving at the same speed as the liquid flow ahead of the bubble, essentially fixing the bubble and allowing the liquid to flow around it [2,14,15,26]. While this approach results in a far smaller domain and, hence mesh, it has drawbacks. For example, the change in hydrostatic pressure around the bubble as it rises cannot be easily included nor can changes in the pipe geometry, which is key to the present application. So, in the present study the full pipe geometry is included in the flow domain, following the work of James et al. [11].

In recent years, CFD studies using the multiphase, Volume of Fluid (VOF) model have replicated observations from experimental studies, such as bubble rise rate and wake behaviour [2,11,19,26]. Other interface reconstruction schemes have been used to model the gas-liquid interface. For example, Suckale et al. [25] developed a numerical model using a level set method and results suggested that a stable bubble could not be sustained with a Reynolds number of more than 100. This corresponds to a maximum pipe diameter of under 0.01 m for a water-air system which is contradicted by many experimental studies. James et al. [13] questioned whether this discrepancy is the result of a physical instability or a numerical instability and pointed out that the simulations were rendered invalid by numerical divergence. Kang et al. [14] used a front tracking method to successfully simulate the rise of Taylor bubbles in 2D axi-symmetrical pipes but no studies have used this method for 3D Taylor bubbles. Lu and Prosperetti [18] also simulated axi-symmetric Taylor bubbles rising through liquids in a vertical tube. Their model neglected the flow in the gas, and tracked the interface using a set of marker points which were linked by cubic splines.

1.1. Objectives

The objectives of this paper are first to accurately describe the process of a single Taylor bubble passing through a change in pipe diameter using a CFD model, validated against the experimental study of James et al. [12]. Second, the lessons learnt from the validation study will be used to create a model to study the effects of a variation in the angle of expansion, θ. Lastly, a parametric study will also be undertaken to examine at which ratio of the diameter of the lower pipe to that in the expansion that the walls of the upper pipe no longer affect the behaviour of the bubble passing through an angle of expansion of 90°. The rationale behind this final part is that there must be asymptotic behaviour as we go from a very small expansion to an infinitely large one.

2. Numerical model

2.1. Governing equations

In this study, a commercial CFD solver, ANSYS FLUENT 14.0, is used. The software uses the finite volume method to solve the momentum and continuity equations. The continuity equation is derived by applying conservation of mass to a finite volume. The momentum equations (Navier–Stokes Equations) are derived from an application of Newton's Second Law. In the air-water system consider in the present research, the film Reynolds number, Refilm, is firmly in the turbulent regime, which means that the wake will be turbulent. As a result of this, the Unsteady Reynolds-Averaged Navier–Stokes equations (URANS) were used,

$$\frac{\partial \rho}{\partial t} + \nabla.(\rho\,\mathbf{u}) = 0, \tag{1}$$

$$\frac{\partial}{\partial t}(\rho\,\mathbf{u}) + (\mathbf{u}.\nabla)\rho\,\mathbf{u} = -\nabla p + \nabla^2[(\mu + \mu_t)\mathbf{u}] + \mathbf{F}_S, \tag{2}$$

where $\mathbf{u}$ is the velocity, p is the pressure, ρ is the density and μ and μ_t are the dynamic and turbulent eddy viscosities respec-

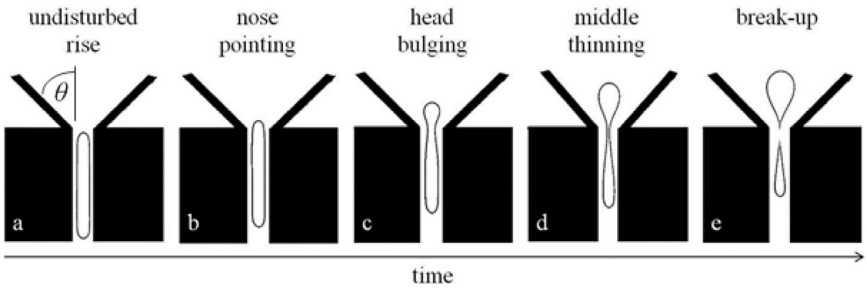

Fig. 7. Diagrams based upon still images taken from a video recording of a Taylor bubble rising through a $\theta = 45°$ expansion, from undisturbed rise (a), through the necking process to breakup (e) (adapted fromSoldati [24]).

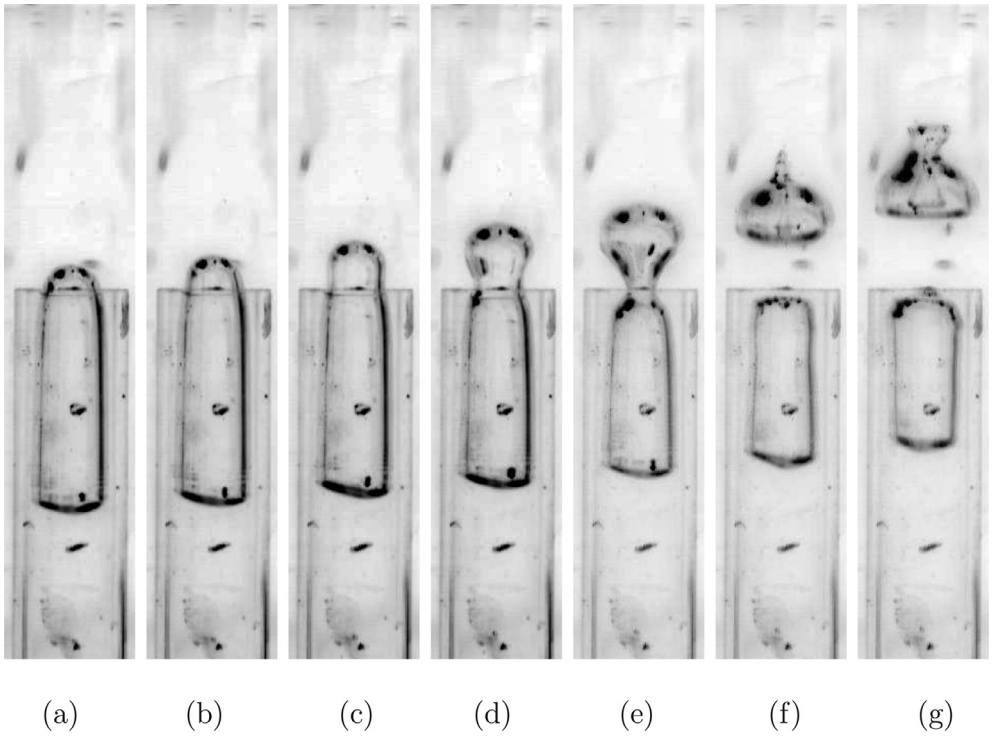

Fig. 8. Negative images taken from high speed video of a Taylor bubble moving from a narrow inner tube into a wider concentric tube (adapted from Carter et al. [5]).

tively and $\mathbf{F}_S$ is the surface tension force. Here, $\mathbf{u}$, p and ρ represent time-averaged quantities.

In the RANS approach whether for single-phase or two-phase systems as we have here, the flow variables, such as pressure, velocity and density, are split into mean and fluctuating components, which are then time averaged. The result of this is that there is an additional term to represent the effects of turbulence in the flow, hence a model is needed to close the equations. Preliminary studies on the air-water system studied here, showed that the Realisable $k-\varepsilon$ (RKE) model [23] is the most suitable turbulence model to use for this application, given the constraints of computational power available.

The rationale for using URANS, an approach that is often criticised by practitioners who use, for example, Large Eddy Simulations (LES) is as follows. First, the computational resources were not available to perform acceptable LES and second, this study was largely concerned with accurately capturing breakup of the bubbles and not, in particular, the wake behind the bubble. While it is clear from the results that we will go on to show that the breakup at the tail of the bubble is not resolved as accurately as it might be using LES and a finer grid, the flow at the nose of the bubble and in the necking region is accurately modelled using our choice of URANS model. However, inaccuracies in the modelling of the wake may result in an error in the rate at which a volume of gas is lost from the bubble at its rear, which will result in a reduction in its length. The loss of gas is due to the formation of small bubbles in the wake. This will be discussed in Section 3.

The RKE model has two transport equations, one for the turbulent kinetic energy, k, and one for the dissipation rate, ε,

$$\frac{\partial}{\partial t}(\rho k) + \nabla.(\rho k\mathbf{u}) = \nabla.\left[\left(\mu + \frac{\mu_t}{\sigma_k}\right)\nabla k\right] + \mu_t S^2 - \rho\varepsilon, \tag{3}$$

$$\frac{\partial}{\partial t}(\rho \varepsilon) + \nabla.(\rho \varepsilon\mathbf{u}) = \nabla.\left[\left(\mu + \frac{\mu_t}{\sigma_\varepsilon}\right)\nabla \varepsilon\right] + C_1\varepsilon S - \rho C_2\frac{\varepsilon^2}{k+\sqrt{\nu\varepsilon}}, \tag{4}$$

where S is the modulus of the mean rate of strain tensor, ν is the kinematic viscosity and σ_k and σ_ε are the turbulent Schmidt numbers. In this model, C_1 is given by

$$C_1 = \max\left[0.43, \frac{\eta}{\eta+5}\right], \tag{5}$$

here $\eta = Sk/\varepsilon$. The remaining model constants, C_2, σ_k and σ_ε have been determined empirically and have values of 1.9, 1.0 and 1.2 respectively. The turbulent eddy viscosity

$$\mu_t = \frac{\rho C_\mu k^2}{\varepsilon}, \tag{6}$$

as in the standard $k-\varepsilon$ model. Here, ρ is the local density as defined in Eq. (13). In the Realisable model C_μ is not a constant but is calculated using the mean strain rate and the rates of rotation, as described in Shih et al. [23].

A multiphase model, capable of producing a distinct interface between the gas and liquid phases, is also required. We use the Volume Of Fluid (VOF) method, which is one of the most common methods to represent the Taylor bubble regime using CFD. This method models the interface by solving a continuity equation for the gas volume fraction, α_G in each cell,

$$\frac{\partial \alpha_G}{\partial t} + \mathbf{u}.\nabla\alpha_G = 0, \tag{7}$$

where α_G is the volume fraction of gas [10]. Here it is assumed that there is no mass transfer between the phases. The liquid volume fraction is then calculated by observing the constraint

$$\alpha_G + \alpha_L = 1, \tag{8}$$

where α_L is the volume fraction of liquid, which must be satisfied to conserve mass. An explicit formulation of the VOF allows the use of a "geometric reconstruction" scheme to reconstruct the interface, based on the "piecewise linear interface calculation" (PLIC) method [28]. This approach does not produce the smearing at the interface seen in other, implicit methods – it does, however, mean that an upper bound is placed on the size of time step that can be used.

Surface tension is approximated by the use of the Continuum Surface Force (CSF) model [3] where a force, $\mathbf{F}_S$ acts at the interface of the two fluids. This is calculated using

$$\mathbf{F}_S = \sigma\kappa\,\mathbf{n}, \tag{9}$$

where σ is the surface tension coefficient, κ is the radius of curvature and $\mathbf{n}$ is the surface normal of the interface, which in terms of the volume fraction, α is

$$\mathbf{n} = \nabla\alpha_{\mathbf{G}}, \tag{10}$$

and κ is given by

$$\kappa = \nabla.\frac{\nabla\alpha_G}{|\nabla\alpha_G|}. \tag{11}$$

To include compressible effects, the air is assumed to be an ideal gas,

$$\rho_G = (p_{\text{atm}} + p)\frac{M_w}{R_0 T} \tag{12}$$

where the operating pressure was taken as atmospheric pressure, p is the static pressure, M_w is the molecular weight of the air, R_0 is the Universal Gas Constant and T is the temperature. The liquid phase is assumed to be incompressible and the flow is assumed to be isothermal.

The density, ρ, and viscosity, μ, that appear in Eqs. (1)–(4) and (6), are constructed from volume fraction-weighted sums of the phase density and viscosity. For example, for the density,

$$\rho = \alpha_G\rho_G + \alpha_L\rho_L, \tag{13}$$

where the notation of Eq. (8) is used.

The PISO algorithm was used throughout to couple the velocity and pressure. While this was originally developed for transient, compressible flows, it can be used for incompressible flows. Indeed, in this two phase application, there are cells in the domain where the local density is the volume fraction-weighted sum of a constant density (the water phase) and a variable density phase (the air). So, we can view the incompressible case as a special case of the compressible case for this multiphase application.

2.2. Domain and mesh

Two domains were required: one for the validation against the work of James et al. [12] (Section 3.1) and one for the study looking at the variation of the angle of expansion (Section 3.2). In all cases, the grid was created in the meshing software ANSYS ICEM-CFD.

For the James study, the domain has a total vertical height of 1.3 m and is based on the experimental apparatus of James et al. [12]. A quarter segment of the domain was used to reduce the computational effort. With reference to Fig. 2(i)–(v), it can be seen that the breakup process exhibits axial symmetry, thus justifying the choice of a quarter segment. The domain is composed of three connected blocks, which are each meshed using a structured, hexahedral mesh. The three blocks are a lower pipe, an expanding section and an upper pipe, shown in Fig. 9(a). The lower pipe is a cylinder of height 0.5 m and internal diameter 0.038 m, and the upper pipe a cylinder of height 0.7 m and internal diameter 0.08 m. Between the upper and lower pipe there is a section of gradually expanding diameter. James, via private correspondence, kindly provided additional photographs of the expanding section used in their experiments which were not presented in James et al. [12]. In the *xy*-plane a standard O-Grid topology as shown in Fig. 9(b) was used.

For the angle of expansion study, a similar approach was used, except for the 90° case, where three blocks were again used but in a different topological arrangement - see Fig. 9(c). Plot (d) in the same figure gives an idea of the aspect ratio of the domain. A long lower section is required for the bubble to stabilize and reach its terminal rise velocity prior to it encountering the expansion. Equally important is a long section above the expansion so as to keep the upper water-air interface sufficiently distance from the expansion zone.

2.3. Initial and boundary conditions

A base case model was created, against which all further simulations except the validation of Section 3.1 were compared. In this base case, the model pipe was initially filled with water to a depth of 5 m with 4.5 m of air above this. A bubble of air was then introduced close to the base of the pipe by specifying the volume fraction of air to be unity in an appropriate region. It is not essential to match the depth of water in the experiments (6 m) to the simulations, because it is the distance of the bubble from the top of the liquid column which is important for bubble dynamics (*ie* a simulated bubble 2 m from the top of a 5 m column behaved the same as a bubble 2 m from the top of a 6 m column of water).

The initial size and shape of the bubble was varied to represent the range of different laboratory experiments performed. The bubble's initial shape for the base case is that of a hemisphere attached to a cylinder with a radius of 0.14 m and length 0.5 m, giving a total length of 0.64 m. This is similar to the bubbles observed in the experiments of Taha and Cui [26]. The initial pressure in the bubble was set at a constant value matching the hydrostatic pressure at the nose of the bubble. The initial velocity field is set to zero everywhere, with very small values, $\mathcal{O}(10^{-5})$, of k and ε also set throughout the domain.

The reference pressure was set as atmospheric (101325 Pa) and was specified at a location which was always within the gas phase above the upper liquid surface. The water surface level was tracked by a User Defined Function (UDF) which determines the maximum level of the water surface at each time-step.

3. Results

3.1. Validation

The vertical position of the nose of the rising bubble was recorded during the simulations. Pressure values were also recorded during the simulations at two measurement points in the domain. These correspond to the locations of the sensors PZ4 and PZ6 from the work of James et al. [12], which were located at the wall at approximately 0.65 m and 0.36 m below the top surface of the liquid as can be seen in Fig. 10. These datasets were then analysed using a Fast Fourier Transform (FFT) to create a power spectral density, from which the dominant frequencies could be determined.

A set of simulations were conducted on grids of 3 different sizes in order to test mesh independence. In these simulations the terminal velocity of the bubble in the lower pipe and frequencies generated as it passed through the expansion were recorded. The GCI method of Celik et al. [6] was used to determine an estimate of the error introduced by spatial discretisation. Meshes of approximately 950,000, 485,000 and 250,000 cells were used, which gave a GCI error of 0.37% for the finest mesh and 0.57% for the intermediate mesh based on the rise velocity in the lower pipe. There was also little qualitative difference in the behaviour of the bubbles as they passed through the expansion section between the cases using the fine and intermediate meshes. It was concluded that the intermediate mesh provided a satisfactory level of accuracy.

A bubble of length 4.4*D* was initialised in the domain, where *D* is the diameter of the pipe below the expansion (0.038 m). The nose of this bubble was initially 0.843 m below the top surface of

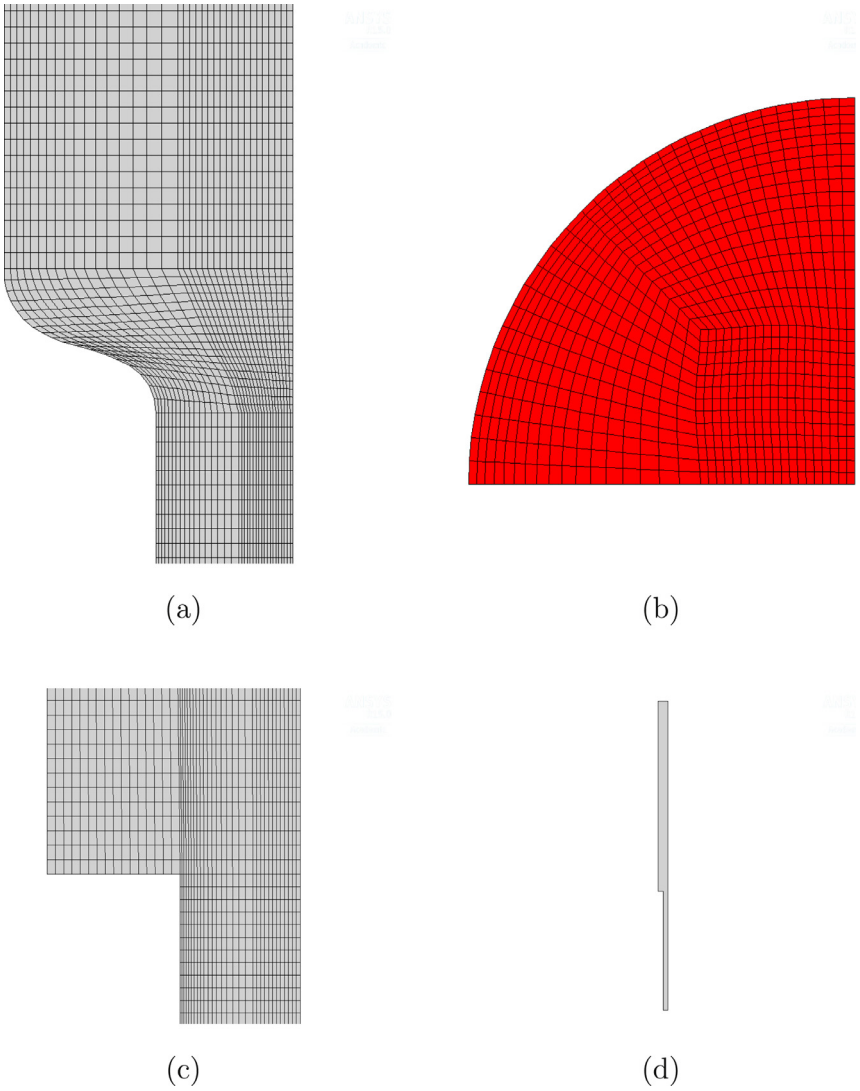

Fig. 9. The surface mesh on (a) a part of the symmetry plane and (b) the outlet on the James et al. [12] domain and (c) on a part of the symmetry plane of the 90° expansion. The full domain for the 90° expansion is shown in (d).

the liquid, and hence 0.243 m below the start of the expanding section. The length of the expanding section was an order of magnitude smaller than the height of water above it. As the bubble ascended the lower tube, a steady rise velocity was quickly reached and maintained. This was followed by a rapid acceleration at the nose as the bubble enters the expanding section, with the bubble typically being split in two. The rise velocity in the lower pipe is within 1.5% of the experimental measurements of James et al. [12], with a corresponding Froude number of 0.355, compared to the experimental value of approximately 0.35.

The frequency analysis revealed dominant frequencies at approximately 13 Hz and 56 Hz, which again are comparable to the frequencies determined in the experiments of James et al. [12] (13 Hz and approximately 56 Hz respectively). The natural frequency of the apparatus that James et al. [12] used was 13 Hz and it was surmised that this was peak was due to an excitation, by fluid processes, of this mechanical mode. That this peak appears at all in our simulations is problematic, since our CFD is static and this fluid-structure interaction cannot possibly take place. However, James et al. [12] do report a second peak at 6 Hz, which they suggest is due to fluid processes and not the excitation of the apparatus. It may, therefore, be that the numerical model here is picking up these low-frequency fluid processes, but not predicting their frequency with accuracy.

The source of these oscillations must be due to the compressibility of the gas phase. It has been reported [1,22] that oscillations are seen in Taylor bubbles in air-water systems, if those bubbles are initially at a pressure not equal to the local hydrostatic pressure at the nose. These lone bubbles are characterised by oscillations in their length as they rise. The natural frequency, w_n of these oscillations is

$$\omega_n = \sqrt{\frac{1}{L}\left[g + \frac{p_{\text{atm}}}{\rho H}\right]} \tag{14}$$

where H is the height of the liquid column above the bubble, L is the length of the bubble, ρ is the density of the liquid phase and g is the acceleration due to gravity. If, at the time of the bubble entering the expansion, it is assumed that the bubble is perturbed, then these oscillations could be initiated. With the initial length of the bubble used here ($4.4D = 0.167$ m) and a height of water above the bubble of approximately 0.6 m, then the frequency of oscillation, $f = \omega_n/2\pi$, is 5.2 Hz. While this is close to the 6 Hz reported by James et al. [12], it should be noted that the models of Pringle et al. [22] and [1] assumed a plug of liquid above the bubble in

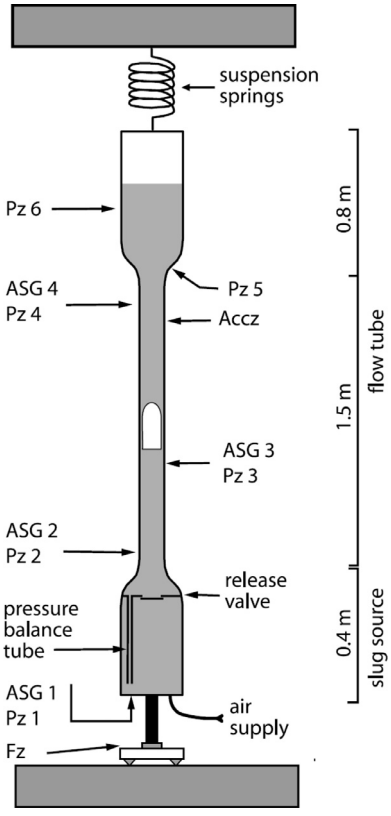

Fig. 10. Experimental apparatus used by James et al. [12].

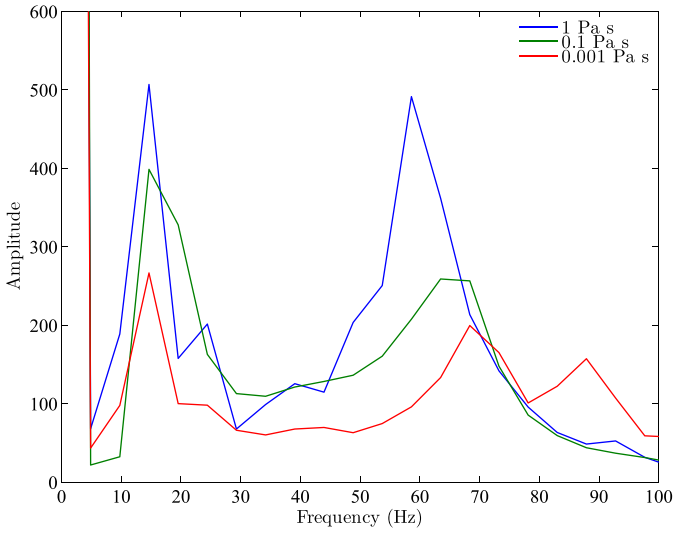

Fig. 11. Plots of the Power Spectral Density of the signals generated by bubbles of identical initial length as they pass through a 90° expansion section for viscosities of 1, 0.1 and 0.001 Pa s respectively.

a pipe of constant diameter. Also, here we have a system, typically, of two bubbles which will form a complex oscillatory system. However, this simple calculation does reveal some insights into the possible source of these low frequency oscillations.

The higher frequency, ~ 56 Hz, was attributed to a short-lived acoustic resonance within the liquid column [12]. While the water was modelled as incompressible, the air phase was not and so it is possible that the bubbly wake behind the Taylor bubble could support these acoustic waves.

Simulations were then conducted with bubble lengths of 2.2D and 3.3D, and these results replicated the behaviour observed in the experiments conducted by James et al. [12]. Inasmuch as the bubble of length 2.2D successfully passed through the expansion before the neck closed, whereas a bubble of length 3.3D was split by the pinching at the neck, which results in a smaller bubble being left behind in the lower pipe.

It should be noted that a full, rather than quarter, model of approximately 2 million cells was created. The simulation produced very similar results to the quarter pipe simulations with a Froude number of 0.352 in the lower pipe and dominant frequencies of 12 and 54 Hz. However, the computing time required was too great to consider this a viable option for all simulations and so the quarter pipe model was used for all subsequent simulations.

A set of simulations were conducted in which the viscosity of the liquid phase was varied. The experiments of Danabalan [8], James et al. [12], Soldati [24] suggest that the necking process is governed mainly by the geometry of the expanding section, rather than the viscosity of the fluid. In the present work, the viscosity of the liquid phase was varied from that of water, 0.001 Pa s, to 0.1 Pa s and then 1 Pa s. Both the buoyancy and liquid film Reynolds numbers indicated that the higher viscosity cases are laminar [17,20].

As the viscosity is increased, there is very little perceptible change in the lower frequency peak shown in Fig. 11. The fact that the low frequency peak did not vary with viscosity lends some credence to our use of Eq. (14) to estimate the oscillatory frequency of the bubble as it enters the expansion. The higher frequency peak is seen to shift to lower frequencies as the viscosity of the liquid increases. This reduction in frequency is analogous to the shifting of the natural frequency of a spring-mass-damper system as the critical damping coefficient is increased.

One qualitative change that can be noticed given an increased liquid viscosity is the decrease in bubbles shed from the tail of the Taylor bubble. Bubbles which are shed in the 0.1 Pa s case are seen to coalesce more readily than the 0.001 Pa s case. This is due to the closed wake structure observed behind the Taylor bubble at these reduced Reynolds numbers [20]. Fig. 12 shows a comparison of streamline plots of the wake regions behind rising Taylor bubbles in liquids of 0.001, 0.1 and 1 Pa s. One consequence of this is that any parts of the bubble shed in the 0.001 Pa s case will reduce the length of the bubble, and hence bubbles may have a different length when reaching the expanding section given a different viscosity. In addition, the thickness of the liquid film around the bubble increases, as indicated by Llewellin et al. [17].

The results of these simulations are in agreement with the conclusions of the experimental studies of Danabalan [8], James et al. [12], Soldati [24]. These suggest that while some damping effects may be observed, viscosity does not play a critical role in the breaking mechanism.

3.2. Variation of angle of expansion

An analysis of the results of the studies of Danabalan [8] and Soldati [24] shows that a more gradual expansion between two pipes of differing diameter will change the behaviour of the rising bubble. A parametric study was conducted to assess the effect of varying the angle of expansion, θ, from 15° to 90° in increments of 15°. This angle is defined as shown in Fig. 13 and is consistent with Fig. 7. An initial set of simulations were conducted to investigate the effect of varying the angle of expansion whilst keeping all other parameters constant. Bubbles with an initial length of 4.4D (0.167 m) were introduced, such that the nose is initially at a depth of 0.843 m below the water surface. The diameter of the lower pipe was 0.038 m, expanding into a 0.08 m pipe.

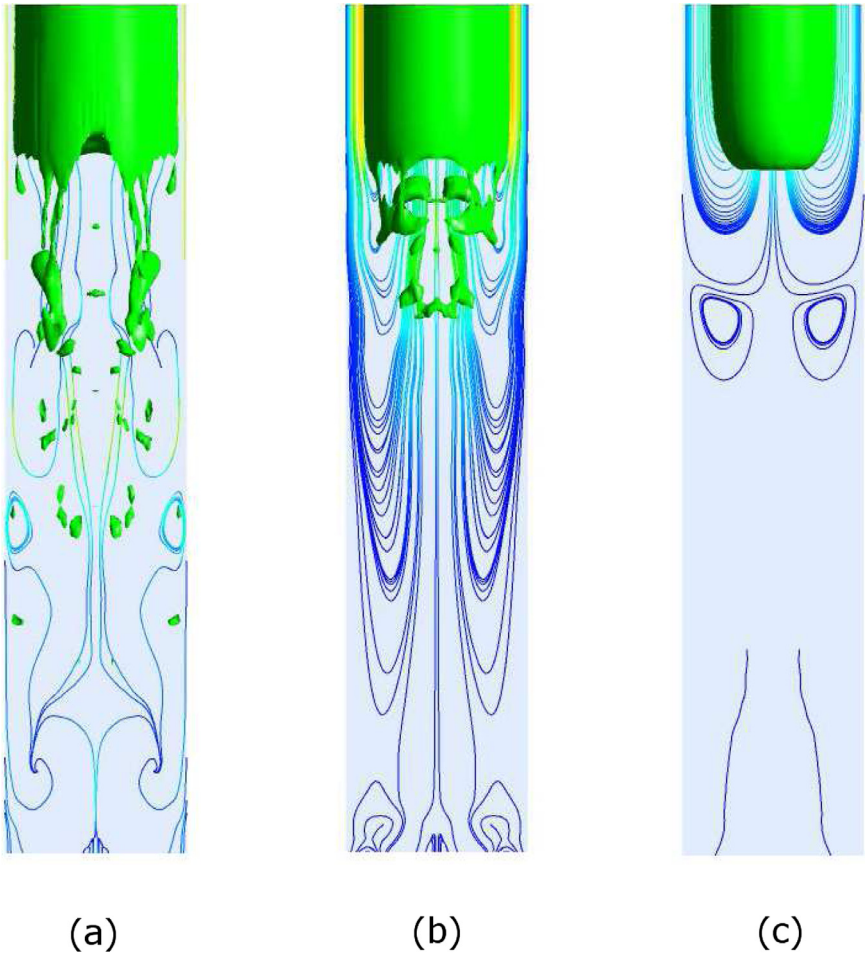

Fig. 12. Plots of the streamlines in the wake of a Taylor bubble rising in fluids of viscosity (a) 0.001 Pa s, (b) 0.1 Pa s, (c) 1 Pa s. Image (a) demonstrates the open wake structure associated with turbulent flow regime given $Re_B > 1500$ [20] and images (b) and (c) demonstrate the closed wake structure associated with the laminar flow regime with $Re_B < 500$.

With this particular length of bubble, as θ is decreased, larger volumes of air are able to pass through the expansion before the bubble splits in two, consequently leaving behind a smaller volume of air in the lower pipe. This effect can be seen in Figs. 14 in which bubbles, all initially the same length, are shown at the same time after release. For higher values of θ the bubbles have already split in two, while at the smaller values they are still intact.

Indeed, we find that for certain lengths of bubble and certain values of θ, the bubble will pass through the expansion largely intact. For a particular value of θ, there will thus be a *critical* bubble length, defined as the maximum length of bubble that will survive the passage intact. Fig. 15 highlights the differences in bubble behaviour for the 90° and 15° cases, once the necking process is complete. For the 90° case, the necking clearly splits the bubble into two distinct daughter bubbles. However, for the 15° case the bubble remains largely intact, leaving only a trail of smaller bubbles in its wake. These two extremes demonstrate clearly a split bubble and an intact bubble.

The "necking" process just referred to is the narrowing of the bubble as it passes through the expansion. Fig. 16 shows that a bubble passing through the 90° expansion expands more quickly in both the lateral and vertical directions because it is not constrained by the walls of the upper pipe. As the liquid passes around the nose of the bubble, its vertical descent is interrupted by the horizontal wall of the expansion and it is directed into the body of the bubble. This flow causes a narrowing or necking of the bubble and ultimately leads to the rupture of the bubble. In the 15° case, the falling liquid film remains largely intact and is merely redirected a little by the wall of the expansion section, resulting in a less dramatic necking.

In order to home in on the critical length for each expansion angle, a further series of simulations were conducted for various lengths of bubble. In each case, the length of the bubble was gradually decreased until it was seen to pass through the expansion intact. This process is not exact and some discretion was required to determine which cases were intact and which were ruptured or split. For example, Fig. 17 shows an example of the simulated upper and lower bounds of the critical length for the 90° expansion case. Thus, it was not possible to identify an exact value for the critical length of the bubble, rather an upper and lower bound. This was partly due to the uncertainty of what constituted an intact bubble and the amount of effort required for each simulation. The shape of the daughter bubble bears a similarity to that seen in Fig. 6 of James et al. [12].

Fig. 18 shows the upper and lower bounds of the critical length against angle of expansion. In the figure, the non-dimensional length, $L' = L_b/D_1$, is used and follows the lead of James et al. [12]. $D_1 (= 2r_1)$ is the lower pipe diameter. It is clear that longer bubbles are able to successfully pass through the smaller angles of expansion. The relationship is not linear and, in fact, a plot of L' against cosec θ reveals a linear relationship (Fig. 19) with R^2 values of 0.998 for the lower bound and 0.997 for the upper bound.

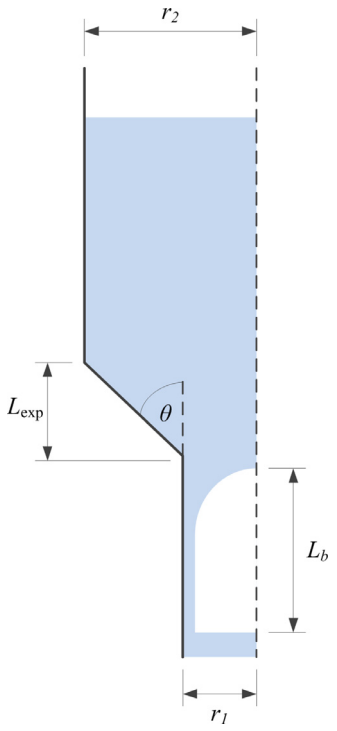

Fig. 13. A schematic of the Taylor bubble approaching an expansion of angle θ. Also, r_1 and r_2 are the radii of the lower and upper pipes respectively, L_b is the length of the bubble and L_{exp} is the length of the expansion.

To quantify this behaviour, the angle, ϕ, of the velocity relative to the vertical axis, was averaged over the radius of the film at the lowest point of the expansion. The angle is

$$\phi = \tan^{-1}\frac{u_r}{u_z} \tag{15}$$

where u_r and u_z are the radial and axial components of the velocity, as indicated in Fig. 20. Fig. 21 demonstrates a linear relationship between ϕ and θ. Clearly, the relationship will change as the bubble passes and the extent of the necking increases, but this is a interesting insight nonetheless.

Some insight into the splitting process can be garnered from arguments based purely on continuity either side of the expansion. Consider, firstly, the time taken for the bubble to rise through the expansion. Assuming a bubble of length, L_b is rising at a speed, w_b, then the time, t_1, taken for the bubble to pass through the expansion is

$$t_1 = L_b/w_b. \tag{16}$$

The rise speed can be recovered from the Froude number,

$$\mathrm{Fr} = \frac{w_b}{\sqrt{gD}}, \tag{17}$$

which for Taylor bubbles for an air-water system takes a value of 0.351 [9]. For a bubble in a uniform cylindrical tube, continuity suggests that the vertical velocity component of the falling water film, w_f^l, well below the nose region, is

$$w_f^l = w_b\left(\frac{r_b^2}{r_1^2 - r_b^2}\right), \tag{18}$$

where r_1 is the radius of the lower pipe (Fig. 13) and the superscript ^{l} refers to the lower pipe. Let us assume that as the bubble moves into the upper pipe it does not immediately expand appreciably laterally and so, by continuity, the vertical component of the flow around the bubble is,

$$w_f^u = w_b\left(\frac{r_b^2}{r_2^2 - r_b^2}\right), \tag{19}$$

where r_2 is the radius of the upper pipe and ^{u} refers to the upper pipe. This assumes local continuity as the flow around the nose of the bubble is redirected down the side of the bubble that remains in the lower pipe. If we assume that this flow is guided by the wall of the expansion into the body of the bubble, then the radial component of flow is

$$u_r = w_f^u \sin\theta. \tag{20}$$

While it passes through the expansion, the bubble is being squeezed by this radial component of liquid flow in the proximity of the base of the expansion. Assuming this component of the flow works its way into the bubble at a constant rate, this will take a time, t_2, to pinch off the bubble

$$t_2 = \frac{r_b}{w_f \sin\theta}, \tag{21}$$

where r_b is the radius of the bubble. Equating t_1 and t_2 for the bubble of critical length, L_c and rearranging gives

$$L_c = \left(\frac{r_2^2 - r_1^2}{r_1}\right)\mathrm{cosec}\,\theta, \tag{22}$$

where we have assumed $r_1 \approx r_b$. This result is clearly very simplified and includes no reference to the fluid properties. However, if we take the 45° case in Fig. 18, which suggests a critical bubble length of approximately $3D$ or 0.114 m. Eq. (22) predicts a value of 0.092 m, which is surprisingly good agreement for such a simplified model. The agreement, however, becomes worse for the 90° expansion critical lengths of 0.076 and 0.13 m for the simulations and simple model respectively. This clearly casts doubt on the simplified model and suggests more work is required.

The experimental results of [24] were also analysed in the same manner, and are shown in Fig. 22. From this it can be observed that a linear relationship may exist between cosec θ and the critical bobble volume (remember Soldati [24] used a Hele-Shaw cell). However, the fit is not as good as that for the CFD models of the present study. In this case, a linear regression analysis leads to a coefficient of determination, R^2 of 0.97. This reduced level of agreement may be due to the large increments between the different volumes of gas injected during the experiments and the consequent lack of accuracy.

3.3. Variation of upper pipe diameter

A set of simulations was conducted in which the diameter of the upper pipe was varied. The angle of expansion was maintained at 90° and the diameter of the lower pipe was maintained at 0.038 m during these simulations. The purpose of these simulations was to determine the effect of varying the ratio between the diameters of the upper and lower pipes on the critical length of the bubble. It was hypothesised that there would be a critical ratio at which the effect of the walls of the upper pipe played no role in the splitting of the bubble.

In these simulations, the diameter, $D_2 (= 2r_2)$ of the upper pipe was varied from 0.06 m to 0.14 m in increments of 0.02 m, which corresponds to a variation in upper to lower pipe diameter ratios, D_2/D_1, of approximately 1.58 to 3.68.

For the narrowest upper pipe, with $D_2/D_1 = 1.58$, Fig. 23 clearly shows that the critical length of the bubble has increased when compared with the 90° expansion used in Section 3.2 and shown in Fig. 18 where $D_2/D_1 = 2.1$. This suggests that the narrowing of the upper pipe has an effect, allowing longer bubbles through

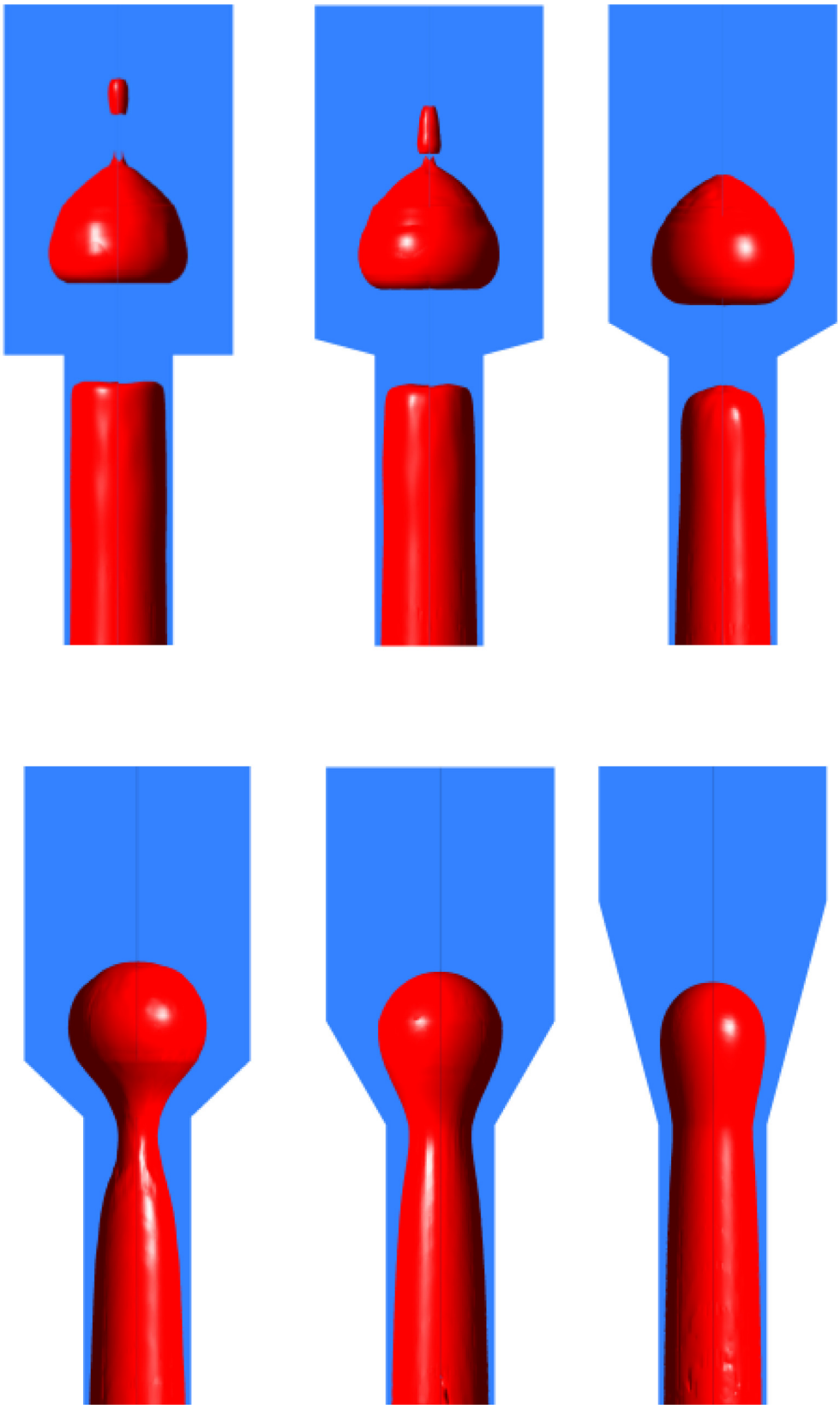

Fig. 14. Iso-surface images indicating the location of initially identical bubbles passing through expansions with angle of expansion, $\theta = 90^{\circ}, 75^{\circ}, 60^{\circ}, 45^{\circ}, 30^{\circ}$and 15° at t = 1.3 s.

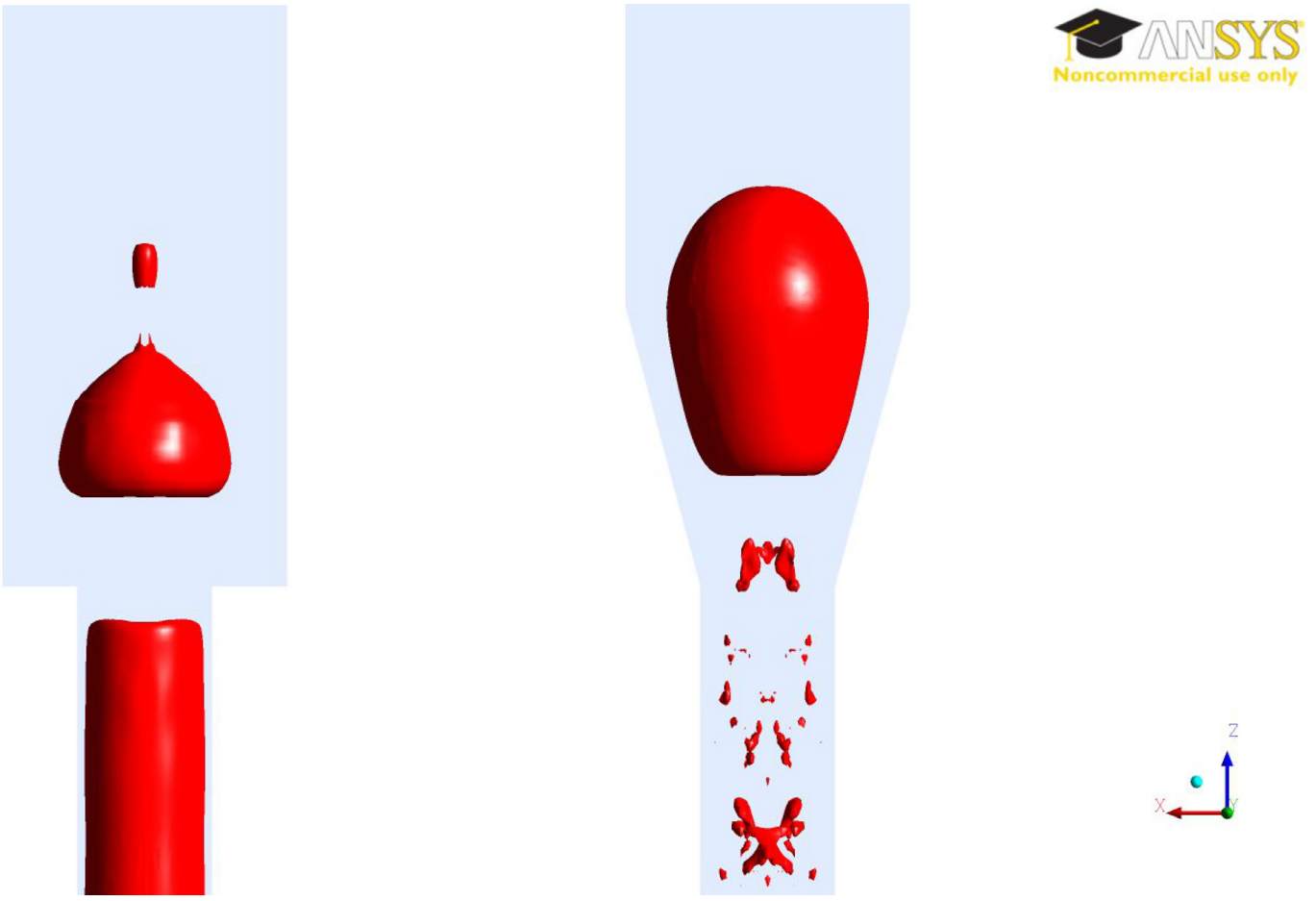

Fig. 15. A comparison between the (a) 90° and (b) 15° cases. Each isosurface indicates the location of the surface of the bubble after the neck has closed.

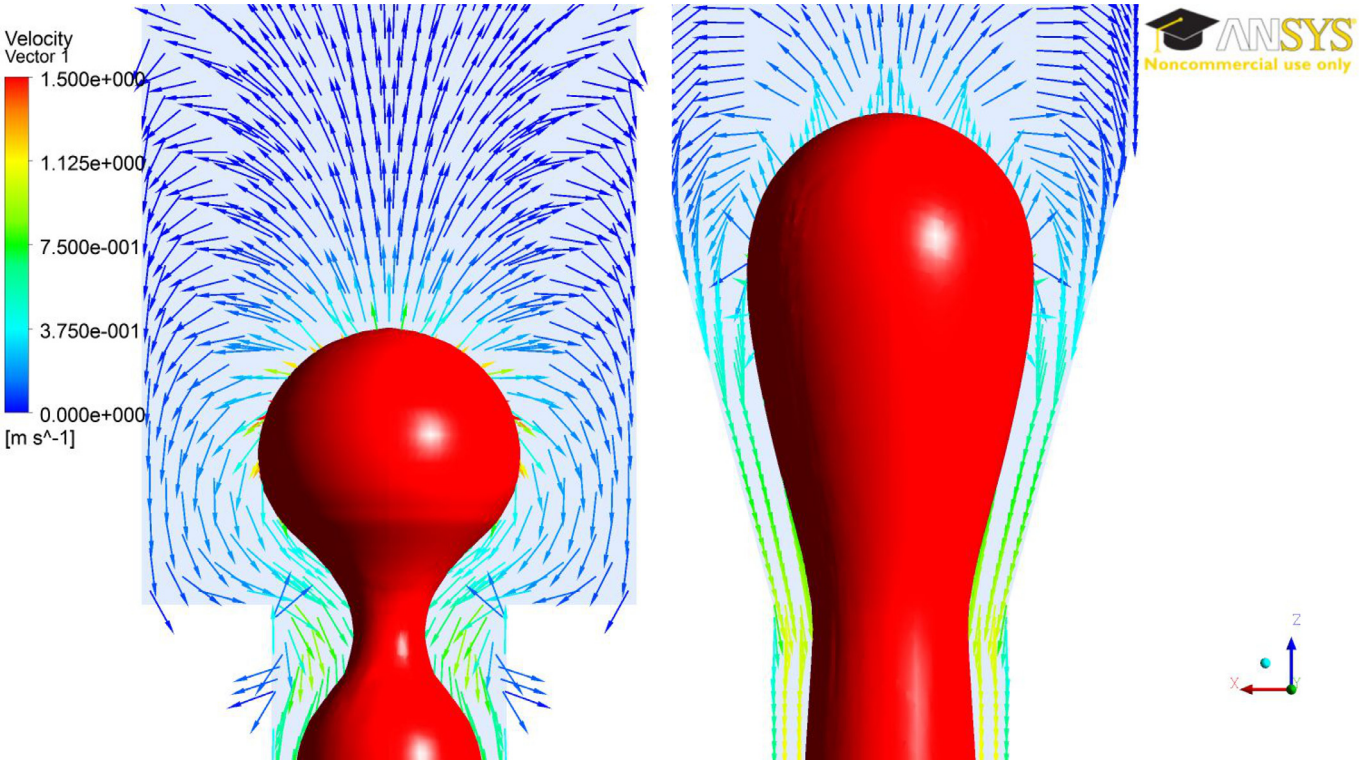

Fig. 16. A comparison between the (a) 90° and (b) 15° cases. For each, the isosurface indicates the location of the surface of the bubble and the vectors represent the velocity.

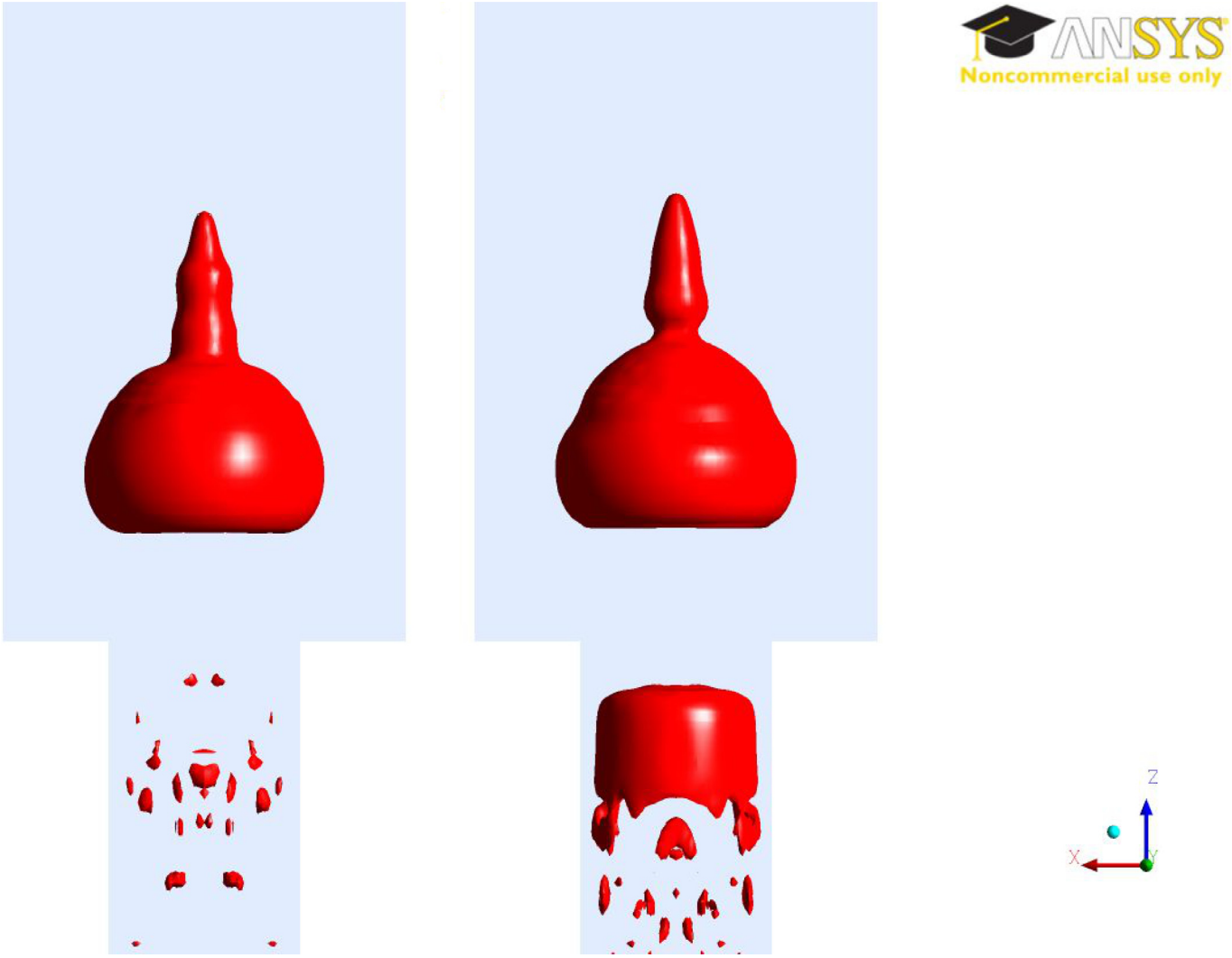

Fig. 17. 3D isosurfaces showing an example of the bubble at or above the upper bound of the critical length(left), and at or below the lower bound of the critical length (right) as they pass through a 90° expansion.

without breakup. It is thought that this is due to a reduced expansion in the head of the bubble. Also, in this case there is a smaller volume of liquid to cause the split in the bubble. As the head of the bubble expands (e.g. Fig. 16(a)), the flow is guided both around the bulging head but also by the wall of the expansion. Both are ultimately key to determining the strength of the radial component that pinches the bubble. It should be clarified that the bubble bulges because the liquid flow governs this process since the air is a relatively passive tracer in the process.

As the ratio D_2/D_1 increases, it can be seen that it is not until the ratio gets above approximately 2.6 that the proximity of the walls of the upper pipe cease to have an effect on the critical length of the bubble. Further, the experiments of Section 3.2 were conducted at ratio below this asymptotic value. It is also noted that at a ratio of 2.6, Eq. (22) performs even more poorly, suggesting that the model works only for smaller D_2/D_1 ratios and lower values of the angle of expansion θ.

4. Conclusions and further work

Firstly, a comprehensive review of the existing literature on Taylor bubble passing through an expansion was presented. It became apparent that there are a number of interesting features of this process. Some bubbles break into smaller parts, others remain largely intact as they pass through the expansion. The bubbles exhibit oscillatory behaviour as they traverse the expansion, resulting in pressure variations in the liquid phase both above and below the expansion.

The qualitative and quantitative behaviour of Taylor bubbles rising through expansions in pipe diameter observed during the laboratory experiments reported by James et al. [12] was modelled using CFD. A frequency analysis of the results of the CFD simulations showed comparable dominant frequencies to the experimental results. The use of a CFD model also confirmed the qualitative mechanism proposed by James et al. [12] for the breaking of a Taylor bubble as it passes through an expansion section.

A variation in the angle of the expansion revealed that much longer bubbles could pass intact through a more gradually expanding section than could through a sudden expansion. All bubbles were seen to “neck” or narrow as they passed through the expansion. The extent of this necking determined whether the bubble would split into two daughter bubbles. A linear variation was found between the critical length of bubble which could pass through the expansion section before the neck closed and the cosecant of the angle of expansion. When analysed in the same fashion, the results of Soldati [24] also exhibited this trend.

A simple model of the necking process, based purely on continuity arguments, was shown to work over a very limited range of

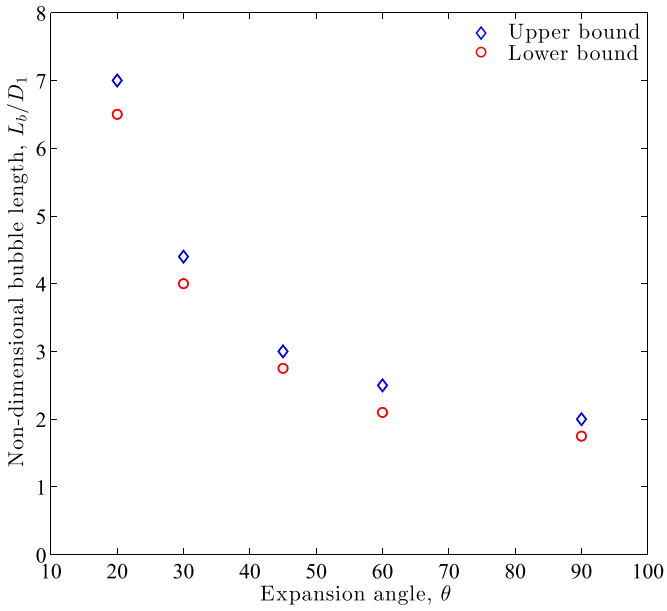

Fig. 18. A plot of the upper and lower bounds of the non-dimensional critical length, L', of bubble against the angle of the expansion.

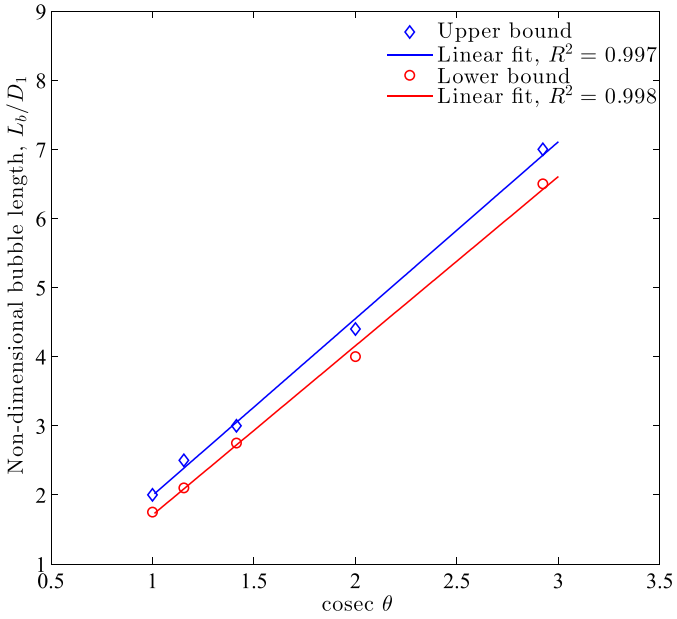

Fig. 19. A plot of the upper and lower bounds of the non-dimensional critical length, L', of bubble against cosec θ.

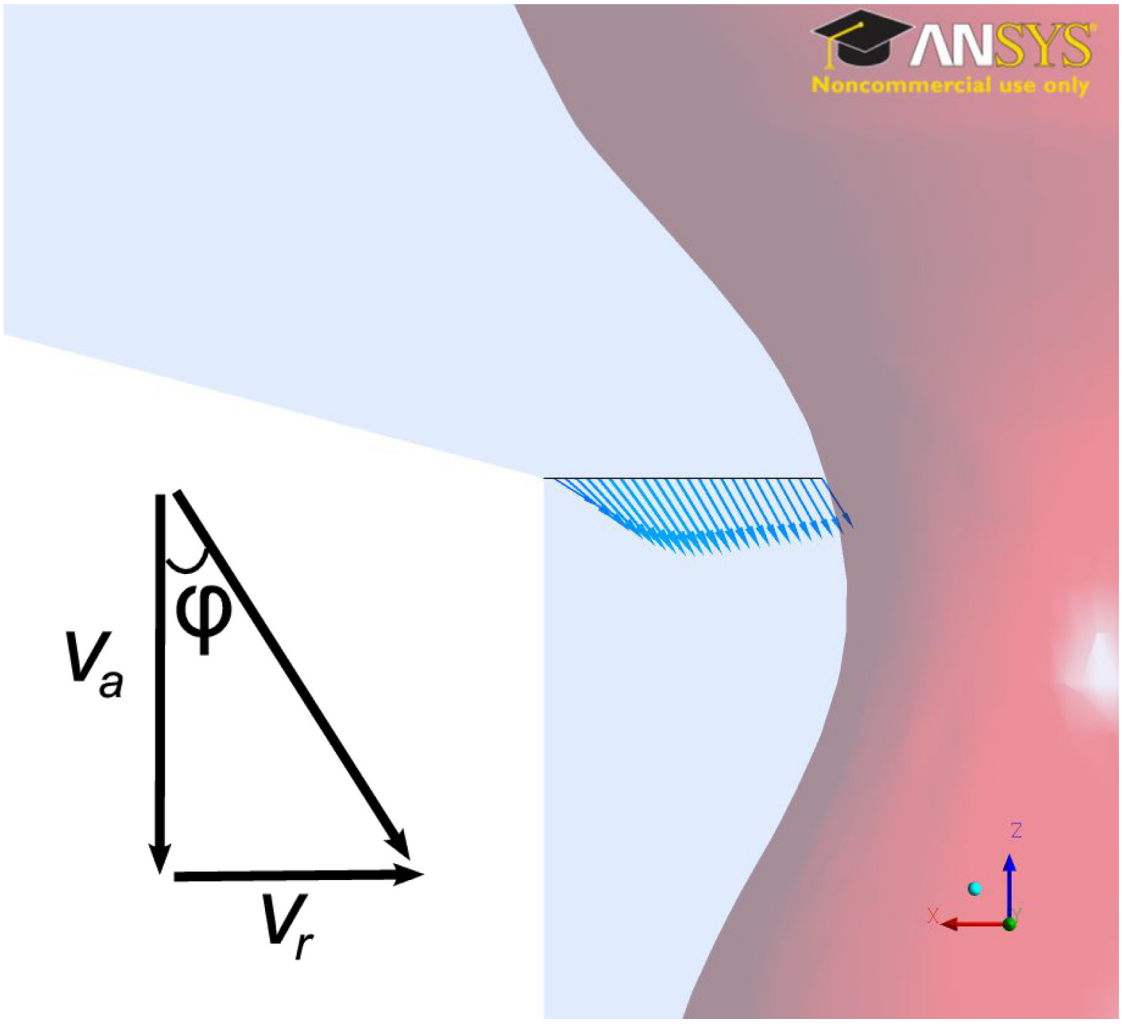

Fig. 20. Schematic illustrating the definition of the angle ϕ.

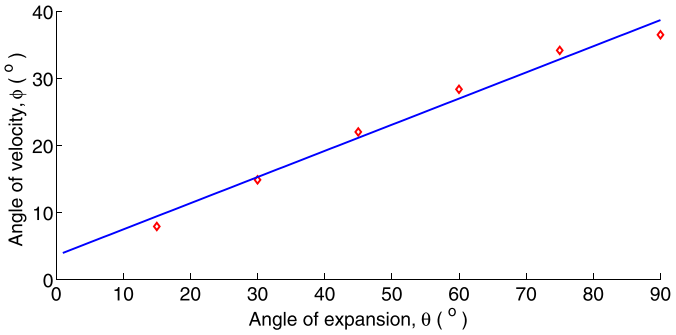

Fig. 21. Plot showing the linear relationship between ϕ and θ.

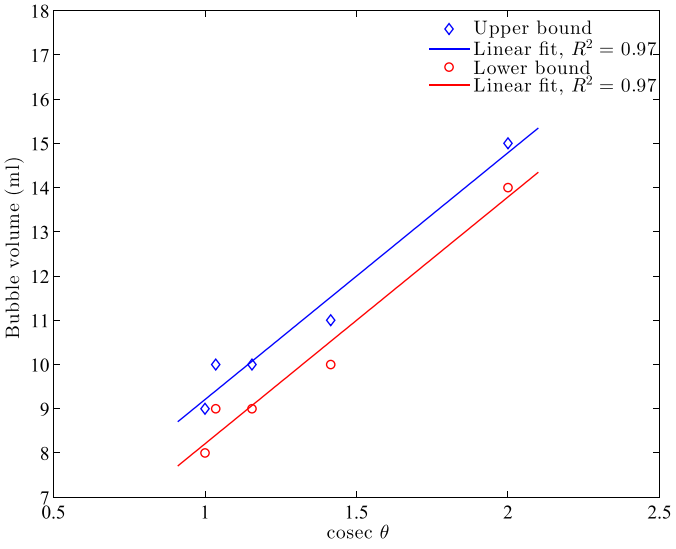

Fig. 22. The upper and lower bounds of the critical volume of bubbles which can fully pass through the expansion before the neck closes against cosec θ for the experiments performed by Soldati [24].

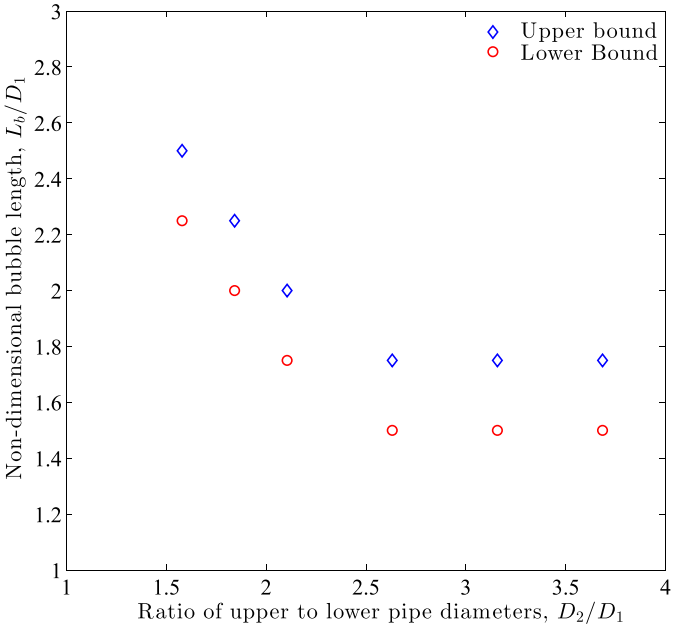

Fig. 23. A plot of the upper and lower bounds of the critical length of bubble against the ratio of the diameter of the upper pipe to the diameter of the lower pipe, D_2/D_1.

angle of expansion, but did at least explain the dependency on the cosecant of the angle of expansion.

For the 90° expansion, the simulations showed that varying the ratio of diameter of the upper pipe to that of the lower pipe did result in a variation in the critical length of bubble that could pass through the expansion intact. At lower ratios, longer bubbles would remain intact. However, as the ratio of upper to lower pipe diameters was increased beyond approximately 2.6, the effect of the walls of the upper pipe ceased.

The majority of the simulations were conducted using an air-water system and there is considerable scope for analysing liquids of different viscosities to examine the range of applicability of these findings.

Acknowledgements

We would like to thank the NERC for funding this research under grant NE/G016593/1. In addition, the authors would like to acknowledge the use of the High Performance Computer at the University of Nottingham.

References

[1] Ambrose S, Hargreaves DM, Lowndes IS. Numerical modeling of oscillating taylor bubbles. Eng Appl Comput Fluid Mech 2016;10(1):578–98.
[2] Araujo JDP, Miranda JM, Pinto AMFR, Campos JBLM. Wide-ranging survey on the laminar flow of individual taylor bubbles rising through stagnant Newtonian liquids. Int J Multiphase Flow 2012;43:131–48.
[3] Brackbill JU, Kothe DB, Zemach C. A continuum method for modeling surface tension. J Comput Phys 1992;100:335–54.
[4] Brown R. The mechanics of large gas bubbles in tubes. Can J Chem Eng 1965;43:375–90.
[5] Carter W, Azzopardi BJ, Agunlejika EO. Taylor bubble destruction at sudden expansions. In: 9th International Conference on Multiphase Flow; 2016.
[6] Celik IB, Ghia U, Roache PJ, Freitas CJ, Coleman H, Raad PE. Procedure for estimation and reporting of uncertainty due to discretization in CFD applications. J Fluids Eng, Trans ASME 2008;130(7).
[7] Clanet C, Héraud P, Searby G. On the motion of bubbles in vertical tubes of arbitrary cross-sections: some complements to the dumitrescu–taylor problem. J Fluid Mech 2004;519:359–76.
[8] Danabalan D. New insights into bubble-driven convection in lava lakes. University of Bristol Master's Thesis 2012.
[9] Dumitrescu DT. Strmung an einer luftblase im senkrechtenrohr. Zeitschrift fr Angewandte Mathematik and Mechanik 1943;23(3):139–49.
[10] Hirt CW, Nichols BD. Volume of fluid (VOF) method for the dynamics of free boundaries. J Comput Phys 1981;39:201–25.
[11] James MR, Lane SJ, Corder SB. Modelling the rapid near-surface expansion of gas slugs in low-viscosity magmas. Geol Soc, London, Special Publ 2008;307(1):147–67.
[12] James MR, Lane SJ, Chouet B. Gas slug ascent through changes in conduit diameter: laboratory insights into a volcano-seismic source process in low-viscosity magmas. J Geophys Res 2006;111.
[13] James MR, Llewellin EW, Lane SJ. Comment on : it takes three to tango: 2. bubble dynamics in basaltic volcanoes and ramifications for modelling normal strombolian activity. J Geophys Res 2011;116.
[14] Kang C, Quan S, Lou J. Numerical study of a Taylor bubble rising in stagnant liquids. Phys Rev E 2010;81.
[15] Kawaji M, DeJesus JM, Tudose G. Investigation of flow structures in vertical slug flow. Nucl Eng Des 1997;175:37–48.
[16] Kondo K, Yoshida K, Matsumoto T, Okawa T, Kataoka I. Flow patterns of gas-liquid two-phase flow in round tube with sudden expansion. In: 10th International Conference on Nuclear Engineering; 2002. p. 179–86.
[17] Llewellin EW, Del Bello E, Taddeucci J, Scarlato P, Lane SJ. The thickness of the falling film of liquid around a taylor bubble. Proc R Soc A 2011;468:1041–64.
[18] Lu X, Prosperetti A. A numerical study of Taylor bubbles. Ind Eng Chem Res 2008;48(1):242–52.
[19] Ndinisa NV, Wiley DE, Fletcher DF. Computational fluid dynamics simulations of Taylor bubbles in tubular membranes model validation and application to laminar flow systems. Chem Eng Res Des 2005;83:40â;;49.
[20] Nogueira S, Riethmuler ML, Campos JBLM, Pinto AMFR. Flow in the nose region and annular film around a Taylor bubble rising through vertical columns of stagnant and flowing newtonian liquids. Chem Eng Sci 2006;61(2):845–57.
[21] Nogueira S, Riethmuller ML, Campos JBLM, Pinto AMFR. Flow patterns in the wake of a Taylor bubble rising through vertical columns of stagnant and flowing Newtonian liquids: An experimental study. Chem Eng Sci 2006;61:7199–212.
[22] Pringle CCT, Ambrose S, Azzopardi BJ, Rust AC. The existence and behaviour of large diameter taylor bubbles. Int J Multiphase Flow 2015;72:318–23.
[23] Shih TH, Liou WW, Shabbir A, Yang Z, Zhu J. A new $k-\varepsilon$ eddy viscosity model for high reynolds number turbulent flows. Comput Fluids 1995;24(3):227–38.

[24] Soldati A. Bubble rise and break up in volcanic conduits. University of Pisa Masters Thesis 2013.
[25] Suckale J, Nave JC, Hager BH. It takes three to tango: 1. simulating buoyancy-driven flow in the presence of large viscosity contrasts. J Geophys Res 2010;115.
[26] Taha T, Cui ZF. Hydrodynamics of slug flow inside capillaries. Chem Eng Sci 2004;59(6):1181–90.
[27] Taylor GI, Davies RM. The mechanics of large bubbles rising through extended liquids and through liquids in tubes. Proc R Soc Lond 1950;200:375–90.
[28] Youngs DL. Time-dependent multi-material flow with large fluid distortion. In: Numerical Methods for Fluid Dynamics. New York: Academic Press; 1982. p. 273.